

pubs.acs.org/cm Article

Room-Temperature Synthesis of Intermetallic Cu-Zn by an Electrochemically Induced Phase Transformation

Yunfei Wang and Anthony Shoji Hall*



Cite This: Chem. Mater. 2021, 33, 7309-7314



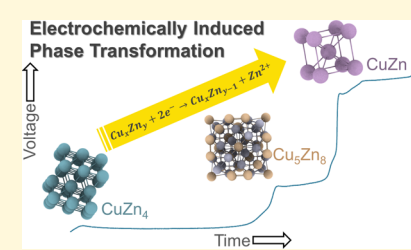
ACCESS

III Metrics & More

Article Recommendations

Supporting Information

ABSTRACT: Ordered intermetallic compounds (OICs) are useful materials for applications ranging from catalysis to optoelectronics. However, generalizable synthetic methods for preparing OIC nanomaterials composed of an electropositive metal and late transition metal has remained a substantial challenge. Herein, we report a process for synthesizing ordered intermetallic γ -Cu₅Zn₈ or intermetallic β -CuZn (high-temperature phase) from Zn-rich Cu alloys at room temperature and atmospheric pressure by an electrochemically induced phase transformation (EIPT). In the EIPT process, Zn is dissolved from the lattice by electrochemical corrosion, initiating the reorganization of the crystal to an intermetallic phase. The transformation of ϵ -CuZn₄ (space group: $P6_3/mmc$)



to ordered intermetallic γ -Cu₅Zn₈ (space group: $\overline{I43m}$) or intermetallic β -CuZn (space group: $\overline{I43m}$) is controlled by the potential and electrolyte used during dealloying. The phases that were accessed was gated by the thermodynamic stability of Zn-rich Cu alloys in aqueous electrolytes. These results have established a key development in the synthesis of intermetallic nanomaterials at room temperature and atmospheric pressure.

1. INTRODUCTION

Ordered intermetallic compounds (OICs) with tailored crystalline structure and morphology are crucial for constructing materials with improved properties for applications ranging from catalysis to optics. ^{1–14} Typically, high temperature and/ or pressure is required for the constituent atoms to interdiffuse and equilibrate into crystals with long-range atomic ordering. However, this is difficult to achieve by conventional lowtemperature synthetic methods such as colloidal synthesis. Furthermore, producing controlled compositions of OICs that contain elements with large differences in reduction potential is challenging. 15,16 For example, Zn(II) has a reduction potential which is ~ 1 V more negative than many active metal ions (e.g., Au, Pd, Cu, Pt, etc.); therefore, it is difficult to co-reduce both elements at controllable rates. ^{15–17} To address this problem, Cable and Schaak et al. developed a two-step synthetic method in which organozinc cations were reacted with preformed noble metal nanoparticles. 15 This strategy produced ordered phases of M-Zn (where M = Au, Cu, and Pd) but with poor control over the particle size and morphology. Furthermore, the precursors used to prepare the noble metal seeds impacted the intermetallic phases obtained. For example, gold nanoparticles prepared from AuCl₂ produced Au₃Zn, while those from Au(CH₃COO⁻)₃ produced AuZn. The underlying reason for the precursor dependence has not been clarified. Moreover, the ratio of zinc cations required to obtain a specific composition was not stoichiometric. These unexplained phenomena make it difficult to rationally extend this method to other compositions and alloy systems. Recently, Janiak et al. used microwave irradiation to prepare Cu-Zn intermetallic phases from metal amidinate precursors and ionic liquid

solvents.¹⁸ While this method was able to produce two different intermetallic phases, it is not economical because it utilized toxic and expensive reagents. A recent study by Skrabalak et al. has shown that intermetallic nanoparticles can exhibit size-dependent disorder-to-order phase transformations, which makes it difficult to simultaneously control the phase and size of the nanomaterial.¹⁹ Synthesizing nanostructured OICs, particularly for alloys consisting of an oxophilic metal and late transition metal, remains a major challenge.

A synthetic method which does not need to rely on the reduction kinetics of the metal-ion precursors could provide improved control of the composition. Recently, we found that ordered intermetallic PdBi₂ could be converted to ordered intermetallic Pd₃Bi at room temperature and atmospheric pressure by electrochemically removing Bi from the crystal.²⁰ The EIPT of a base metal-rich alloy to an alloy richer in a nobler metal does not rely on the reduction kinetics to control the phase; instead, thermodynamic stability regulated the structural evolution. Inspired by this approach, we hypothesized that EIPTs could be a promising method for preparing intermetallic compounds with controlled composition among elements with large differences in reduction potential. Herein,

Received: May 16, 2021 Revised: August 19, 2021 Published: September 8, 2021





we demonstrated that EIPTs can be used to prepare ordered intermetallic γ -Cu₅Zn₈ and intermetallic β -CuZn phases at room temperature using ϵ -CuZn₄ or η -Cu_{0.05}Zn_{0.95} alloys (which are easily accessible phases) as precursors. As Zn was removed from Zn-rich alloys, the crystal reorganized to ordered intermetallic γ -Cu₅Zn₈ or intermetallic β -CuZn, depending on the potential and electrolyte composition. The observation that Zn-rich Cu alloys undergo an EIPT is consistent with our hypothesis that low-melting-point materials can exhibit considerable interdiffusion of the constituent elements at room temperature during dealloying. 20–22 To the best of our knowledge, we are not aware of other methods for preparing γ -Cu₅Zn₈ and β -CuZn at room temperature and atmospheric pressure in aqueous media. Intermetallic Cu-Zn materials with improved control over composition and morphology may enable improved performance for applications in electrochemical CO2 reduction and as anodes for Limetal batteries. The EIPT process avoids the use of strong reducing agents, which are often toxic, and can be performed in aqueous electrolytes. Furthermore, the composition and phase of the material can be rationally tuned since the reduction kinetics of Cu and Zn cations are uncoupled; instead, our method relies on electrochemical stability for isolating the desired phase.

2. EXPERIMENTAL SECTION

- **2.1. Materials.** Cu foam (MTI Corporation), Acetic Acid (CH₃COOH, ACS Grade, Fisher Chemical), Potassium Hydroxide (KOH, 99.99%, Alfa Aesar), Sodium Sulfate (Na₂SO4, anhydrous, 99.99%, Alfa Aesar), Glycine(C₂H₅NO₂, 99+%, Alfa Asar), Copper-(II) Sulfate Hydrate (CuSO₄ \bullet xH₂O, 99.999%, Alfa Aesar), Hg/HgO electrode (CHI 152), Hg/HgSO₄ (CHI 151), Zinc Sulfate Hydrate (ZnSO₄ \bullet 7H₂O, 99.0–103.0%, Alfa Aesar), and Electroplating Tape (3M) were used as received. Deionized water was purified by a Millipore water purification system (resistance: 18.2 M Ω) was used without further purification. Ag foil (99.9%, Alfa Aesar) was polished with 1200 grit sandpaper followed by 2000 grit sandpaper before use. Cu foam (MTI Corp) was used as received.
- **2.2. Electrochemical Setup.** Potentiostats from Pine Research and Metrohm were used to control the applied potential. A Pt mesh was used as the counter electrode. A Teflon cell and Hg/HgO electrode filled with 1 M KOH were used to perform experiments in alkaline electrolytes. A glass cell and Hg/HgSO $_4$ filled with saturated Na $_2$ SO $_4$ solution were used for experiments in neutral or acidic electrolytes.
- **2.3.** Electrodeposition of ϵ -CuZn₄ and Cu, Zn, on Ag Foil. ϵ -CuZn₄ was electrodeposited on Ag foil with a surface area of 1.2×1.5 cm². The electrolyte was prepared by dissolving 1.064 g of CuSO₄ (0.0066 mol), 6.71 g of ZnSO₄•7H₂O (0.0233 mol), 8.75 g of C₂H₅NO₂ (0.117 mol), and 10.7 g of Na₂SO₄ (0.033 mol) into 100 mL of deionized water. After stirring for 10 min, the pH was adjusted to 9.5 by adding KOH. The solution was sonicated for 10 min before each experiment The ϵ -CuZn₄ samples were deposited at -1.4 V versus Hg/HgO for 1600 s. Electrodeposition of Cu and Zn was performed in a solution that only contained precursors of the targeted metal.
- **2.4. Electrodeposition of** ϵ -CuZn₄ **on Cu Foam.** ϵ -CuZn₄ was electrodeposited on Cu foam with a geometric surface area of $1.2 \times 1.2 \text{ cm}^2$. Both sides of the Cu foam were exposed to the electrolyte in all experiments. The ϵ -CuZn₄ was deposited galvanostatically at -130 mA for 300 s. The measured potential was around -1.65 V versus the Hg/HgO reference electrode.
- **2.5.** Dealloying of ϵ -CuZn₄ on Ag Foil in an Acid. Dealloying was performed in a solution containing 2.871 mL of CH₃COOH (0.05 mol), 8.05 g of Na₂SO₄ (0.025 mol), and 25 mL of deionized water. After stirring for 15 min, deionized water was added until the total volume reached 100 mL. The pH of the solution was adjusted to

- 5 by adding KOH pellets. The electrochemical cell was heated in a water bath to 30 $^{\circ}$ C before dealloying. Galvanostatic dealloying was conducted by applying a current density of 0.75 mA cm⁻².
- **2.6.** Dealloying of ϵ -CuZn₄ on Ag Foil in an Alkaline Solution. A total of 5.6 g of KOH (0.1 mol) was added into 100 mL of deionized water. The water bath, counter electrode, and galvanostatic dealloying procedure were the same as that described for dealloying in acidic solutions.
- **2.7.** Dealloying of ϵ -CuZn₄ on Cu Foam. Dealloying of ϵ -CuZn₄ on Cu foam was similar to dealloying on Ag foil in both alkaline and acidic solution, except the current was adjusted to 0.4 mA
- **2.8. Characterization.** The crystal structure of materials was characterized by powder X-ray diffraction (PXRD). The samples were prepared by scratching off a thin film onto Kapton tape. A Philips X'Pert Pro Powder X-ray diffractometer was used with Cu K radiation (K α_1 , $\lambda=1.5406$ Å; K α_2 , $\lambda=1.5444$ Å). Crystallographic Information File (CIF) was downloaded from the Inorganic Crystal Structure Database (ICSD). Simulated XRD patterns were calculated from VESTA ver. 3.5.7.

Scanning electron microscope (SEM) images were taken on an a MIRA3 TESCAN electron microscope at 10.0 kV in the SE mode.

X-ray photoelectron spectroscopy (XPS) spectra were collected on a PHI 5600 XPS (58.7 eV pass energy, 0.250 eV/step, Mg K α X-rays). The samples were prepared by scratching off thin film samples onto the carbon tape attached to a flat substrate. Quantitative analysis was conducted with CasaXPS software.

Inductively coupled plasma mass spectrometry (ICP-MS) was conducted on a PerkinElmer NexION 300D with ICP. The samples were first scratched off from the substrate into a plastic tube. Then, 10% nitric acid was added into the tube to dissolve the materials. External calibration was conducted before each measurement with standardized solutions.

3. RESULTS AND DISCUSSION

We studied the dealloying behavior of intermetallic ϵ -CuZn₄ thin films prepared by electrochemical deposition.²³ The crystal structure and composition of the material were probed by XRD, ICP-MS, and XPS. The XRD pattern of the electrodeposited material was assigned to ϵ -CuZn₄, the most dominant peak was the (002) plane; suggesting that the sample was textured along the [001] orientation (Figure S1a). The atomic ratio of the thin film was ~89% Zn and 11% Cu, which was 1% higher than the most Zn-rich composition of ϵ -CuZn₄, suggesting that the deposited material was supersaturated with Zn (Table S1a). High-resolution XPS showed the presence of metallic Cu and Zn as indicated by the Cu 2p_{3/2} peak at 933.3 eV, Cu 2p_{1/2} peak at 953.2 eV, and Zn 2p_{3/2} peak at 1022.7 eV (Figure S2). ϵ -CuZn₄ was found to produce films with a thickness of \sim 48 μ m; the material was composed of fused layers of fractal-like Cu islands which formed pores that penetrated throughout the thickness of the film (Figure S1b,c). It is worth noting that we attempted to prepare β -CuZn and γ -Cu₅Zn₈ directly by tuning the voltage used during electrochemical deposition; however, these phases were not isolated in the phase-pure form (Figure S3). This is consistent with the literature reports which have shown that intermetallic β -CuZn and ordered intermetallic γ-Cu₅Zn₈ cannot be directly prepared in pure form by electrochemical deposition from aqueous electrolytes. $^{23-25}$

Pourbaix diagrams were used to evaluate the thermodynamic stability of ϵ -CuZn₄ in aqueous electrolytes (Figure 1a). The Pourbaix diagram showed that three phases can be accessed by an EIPT: γ -Cu₅Zn₈, β -CuZn, and Cu. The low melting point of ϵ -CuZn₄ (\sim 500 °C) suggested that atoms will reorganize during Zn dissolution, enabling the formation of γ -Cu₅Zn₈ and

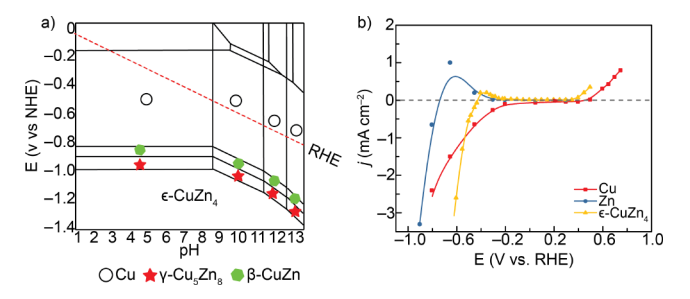


Figure 1. (a) Pourbaix diagram of ϵ - CuZn₄ showing the stability of solid metallic phases. The oxide phases and dissolved ions were removed from the diagram for clarity. The Pourbaix diagram was adapted from materialsproject.org for ϵ -brass. (b) Steady-state current vs voltage diagram of Cu, Zn, and ϵ -CuZn₄ electrodes at pH 5.

 β -CuZn at room temperature and atmospheric pressure. The corrosion behavior of ϵ -CuZn₄ was assessed by constructing a current versus voltage diagram under steady-state conditions in a pH 5 solution containing 500 mM CH₃COOH and 250 mM Na_2SO_4 (Figure 1b). When the potential of ϵ -CuZn₄ electrodes was <-0.45 versus RHE, cathodic current caused by the hydrogen evolution reaction (HER) was observed. Two anodic waves were observed, one centered at -0.405 V and the other which onset at 0.395 V. To understand the processes belonging to these anodic features, we evaluated the corrosion behavior of Cu and Zn. Cathodic current corresponding to the HER was observed on Cu and Zn electrodes for potentials <-0.2 and <-0.75 V, respectively. Zn displayed an anodic wave centered at -0.655 V caused by dissolution, and Cu displayed an anodic wave which onset at 0.495 V caused by dissolution. Therefore, we assigned the anodic features on ϵ -CuZn₄ electrodes at -0.405 and 0.395 V to the dissolution of Zn and Cu, respectively. The Zn dissolution potential shifted by 250 mV, which suggested that Zn was stabilized in the lattice of ϵ -CuZn₄.

According to the Pourbaix diagram, γ -Cu₅Zn₈ and β -CuZn are more stable than ϵ -CuZn₄, and are expected to form between -0.71 and -0.5 V versus RHE (-1 and -0.8 V vs NHE) which overlaps with the HER (Figure 1a). According to our experimental corrosion diagram, the EIPT should occur between -0.425 and 0.2 V versus RHE, where only Zn can dissolve from ϵ -CuZn₄ (Figures 1b and S4). To test this hypothesis, we performed potentiostatic dealloying at 0 V versus RHE (Figure 2a). Initially, a large anodic current of 4 mA cm⁻² was observed, presumably from Zn dissolution, before decreasing to 0 mA cm⁻² after ~1500 s (Figure 2b). The crystalline structure of the dealloyed material was evaluated by XRD and the resulting pattern was found to

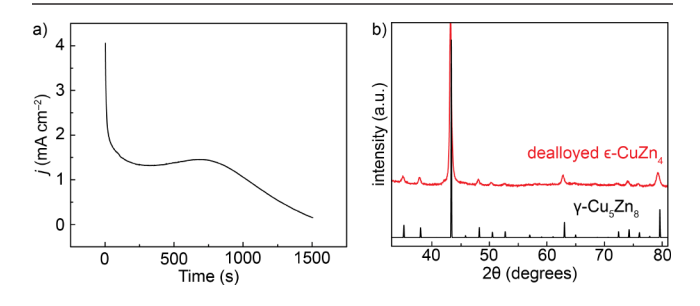


Figure 2. (a) Potentiostatic dealloying of ϵ -CuZn₄ at 0 V vs RHE. (b) XRD pattern of dealloyed ϵ -CuZn₄ which showed that it transformed to γ -Cu₅Zn₈ (ICSD108419).

match with γ-Cu₅Zn₈. The chemical composition was found to be 69% Zn and 31% Cu which was within the expected composition range of γ-Cu₅Zn₈ (Table S1).²⁶ High-resolution XPS scans of γ-Cu₅Zn₈ revealed a binding energy of Cu 2p_{3/2} peak at 933.2 eV, Cu 2p_{1/2} peak at 953.1 eV, and Zn 2p_{3/2} peak at 1022.2 eV; therefore, the oxidation state of Cu and Zn was metallic (Figure S2). Constant potential dealloying at other voltages within the range of -0.35 to 0.2 V versus RHE also yielded γ-Cu₅Zn₈. SEM micrographs revealed that γ-Cu₅Zn₈ displayed the same morphology as the ε-CuZn₄ precursor material (Figure S6). Taken together, these data have demonstrated that ε-CuZn₄ was converted to γ-Cu₅Zn₈ upon the removal of Zn at room temperature and atmospheric pressure.

We explored the phase conversion behavior of $\varepsilon\textsc{-}\mathrm{CuZn_4}$ in more detail by constructing a voltage versus time diagram and monitoring the crystal structure at specific time points (Figure 3a), analogous to how the phase transition behavior of Li-ion

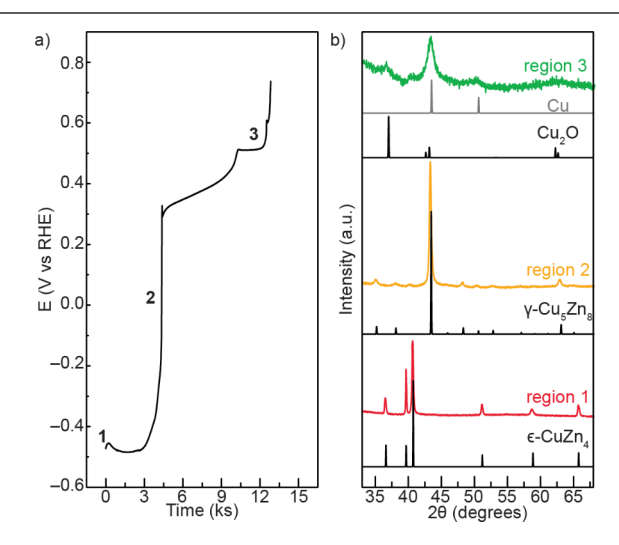


Figure 3. Dealloying of ϵ -CuZn₄ at pH 5 by (a) constant current dealloying at 0.75 mA cm⁻² and (b) XRD of regions 1, 2, and 3 shown in part (a). ϵ -CuZn₄ (ICSD103157) transformed to γ -Cu₅Zn₈ (ICSD108419), before transforming to a mixture of Cu₂O (ICSD190597) and Cu (ICSD43493).

battery anodes is evaluated. 21,27,28 The beginning stage of ϵ -CuZn₄ corrosion formed a plateau centered at -0.47 V versus RHE; upon further dealloying, we observed an additional plateau and two regions where the voltage changed rapidly with time (Figure 3a). Two phases coexist in the plateau region and the width represents the breadth of the miscibility gap between phases; single phase materials were observed in regions where the voltage changed rapidly with time. The crystal structure of the material in the single-phase region (denoted as region 2), which spanned from -0.4 to 0.3 V versus RHE, matched with γ -Cu₅Zn₈ (Figure 3b).

 γ -Cu₅Zn₈ was found to be stable up to \sim 0.30 V versus RHE; above this voltage, it converted to Cu with a small amount of Cu₂O, presumably from oxidation in air (Figure 3). The diffraction peaks of γ -Cu₅Zn₈ were broadened in comparison with the ϵ -CuZn₄ starting material. Williamson—Hall analysis of the XRD diffractograms was used to determine the microstrain and grain size of the materials (Figure S5). As ϵ -CuZn₄ was dealloyed to γ -Cu₅Zn₈, the grain size decreased from \sim 90 to 35 nm and the microstrain decreased from 0.2 to 0.13%, respectively; suggesting that strain was reduced by the

formation of additional grain boundaries during the EIPT. The plateau between region 1 and 2 displayed a mixed-phase material consisting of ϵ -CuZn₄ and γ -Cu₅Zn₈ (Figure S7). It was unclear if a mixed phase was present between regions 2 and 3 since the peaks of Cu and Cu₂O overlapped with γ -Cu₅Zn₈ (Figure S8). We did not observe β -CuZn, even though the Pourbaix diagram suggested that it can be accessed. This implied that β -CuZn was not accessible at pH 5; instead, the direct transformation of γ -Cu₅Zn₈ to Cu was favored. Thus, we conclude that dealloying ϵ -CuZn₄ (region 1) transformed it to γ -Cu₅Zn₈ (region 2) before finally transforming to Cu and/or Cu₂O (region 3).

We hypothesized that any alloy phase which was richer in Zn than $\gamma\text{-}\mathrm{Cu}_5\mathrm{Zn}_8$ could be converted to $\gamma\text{-}\mathrm{Cu}_5\mathrm{Zn}_8$ since the EIPT process is gated by thermodynamic stability. To test this hypothesis, we deposited $\eta\text{-}\mathrm{Cu}_{0.03}\mathrm{Zn}_{0.97}$ and subjected it to galvanostatic dealloying under the same conditions as $\epsilon\text{-}\mathrm{CuZn}_4$ (Figure S9). The $\eta\text{-}\mathrm{Cu}_{0.03}\mathrm{Zn}_{0.97}$ solid solution started to corrode at $\sim\!-0.5$ V versus RHE, which was $\sim\!100$ mV more negative than $\epsilon\text{-}\mathrm{CuZn}_4$; nevertheless, the rest of the diagram was the same (Figures S10 and 3a). Taken together, these data indicated that Cu–Zn alloys with compositions richer in Zn than $\gamma\text{-}\mathrm{Cu}_5\mathrm{Zn}_8$ can reconstruct and form $\gamma\text{-}\mathrm{Cu}_5\mathrm{Zn}_8$ by the EIPT process, indicating that thermodynamics control the evolution of phases.

The preparation of nanomaterials by traditional low-temperature methods is known to be sensitive to the solvent utilized during synthesis. $^{29-33}$ Inspired by this, we interrogated the dealloying of ϵ -CuZn₄ at pH 14 to reveal the dependence of the EIPT process on the solvent composition. To perform this study, ϵ -CuZn₄ (region 1) was galvanostatically dealloyed in a pH 14 electrolyte to construct a voltage versus time diagram (Figure 4a). A plateau at -0.35 V versus RHE preceded a single-phase region (denoted as region 2) which spanned the voltage range -0.35 to -0.1 V versus RHE. The material in this region could be indexed to γ -Cu₅Zn₈ (Figure 4b). After the formation of γ -Cu₅Zn₈, another plateau was observed at -0.1 V which preceded a single-phase region

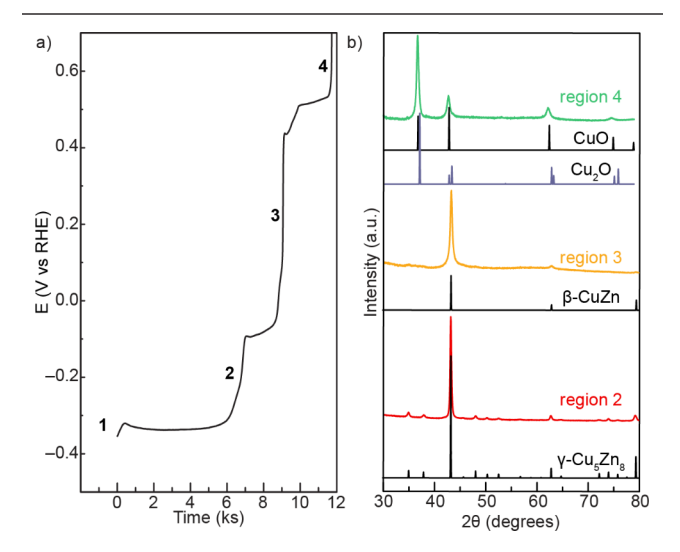


Figure 4. Dealloying of ϵ -CuZn₄ (denoted as region 1) at pH 14 by (a) constant current dealloying at 0.75 mA cm⁻² and (b) XRD of regions 2, and 3, and 4 shown in part (a). ϵ -CuZn₄ (ICSD103157) transformed to γ -Cu₅Zn₈ (ICSD108419) and then β -CuZn (ICSD103152), than to a mixture of Cu₂O (ICSD 190597) and CuO (ICSD 61323).

(denoted as region 3) that spanned from -0.1 to 0.4 V versus RHE. The material in region 3 could be indexed to β -CuZn (high-temperature phase), albeit with a small amount of γ -Cu₅Zn₈ impurity (Figure 4b). Furthermore, the composition of this material was found to be 38.0% Zn and 62.0% Cu which is within the expected composition range of β -CuZn (Table S1). High-resolution XPS showed the presence of metallic Cu and Zn, indicated by the Cu $2p_{3/2}$ peak at 932.8 eV, Cu $2p_{1/2}$ peak at 952.8 eV, and Zn $2p_{3/2}$ peak at 1022.0 eV (Figure S2). SEM micrographs revealed that β -CuZn exhibited a similar morphology to the parent ϵ -CuZn₄ alloy (Figure S11). The diffraction peaks of γ -Cu₅Zn₈ and β -CuZn were broadened in comparison to the ϵ -CuZn₄ precursor. As ϵ -CuZn₄ was dealloyed to γ-Cu₅Zn₈, the average grain size decreased from ~90 to 20 nm and the microstrain decreased from 0.2 to 0.07% (Figure S5). β -CuZn displayed an average grain size of 35 nm and the microstrain 0.31% (Figure S5). A plateau at 0.5 V versus RHE was observed to precede a singlephase region (denoted as region 4) when β -CuZn was dealloyed. XRD of the material in region 4 was assigned to a mixture of Cu₂O and CuO (Figure 4b). The two-phase region preceding plateau 4 was indexed to a mixture of CuO and β -CuZn intermetallic (Figure S12). Taken together, these results have shown that changing the electrolyte from pH 5 to pH 14 had a profound impact on the crystalline phases that were accessed; enabling intermetallic ϵ -CuZn₄ to transform to γ - Cu_5Zn_8 and then to β -CuZn.

Nanostructured coatings of γ -Cu₃Zn₈ and β -CuZn were prepared on Cu foam electrodes to demonstrate that the EIPT method can be used to prepare materials with hierarchical morphologies which would allow the materials to be useful for functional applications. The ϵ -CuZn₄ precursor was coated over the Cu foam by electrochemical deposition. The dealloying of ϵ -CuZn₄ displayed a similar voltage versus time diagram to the planar electrodes in both pH 5 and pH 14 electrolytes, which showed that both δ -Cu₃Zn₈ and β -CuZn phases could be accessed (Figures S13 and 14). The ϵ -CuZn₄ film was found to form a dendritic morphology on the surface of the Cu foam; similar structures were also observed on γ -Cu₃Zn₈ and β -CuZn indicating that the morphology of the parent material was retained (Figure S15).

4. CONCLUSIONS

In conclusion, we have prepared ordered intermetallic γ -Cu_SZn₈ and intermetallic β -CuZn at room temperature and atmospheric pressure by an EIPT of ϵ -CuZn₄ (Figure 5). The EIPT process is gated by the thermodynamic stability of phases in the aqueous electrolytes and is not constrained by kinetics since low-melting-point materials exhibit facile atomic reorganization during dealloying. The composition of the

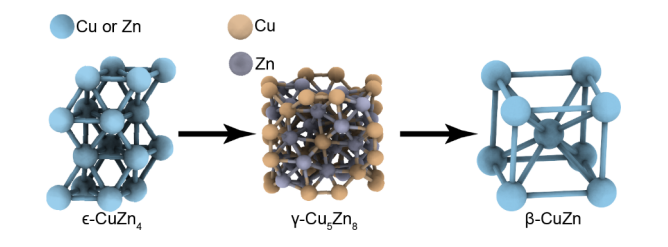


Figure 5. Schematic showing the EIPT of ϵ -CuZn₄ to γ -Cu₅Zn₈ and then to β -CuZn. A 2 × 2 cell is shown for ϵ -CuZn₄, and the unit cells are shown for γ -Cu₅Zn₈ and β -CuZn.

solvent was found to control the number of phases which could be accessed; only $\gamma\text{-Cu}_5Zn_8$ was formed in pH 5 electrolytes, while both $\gamma\text{-Cu}_5Zn_8$ and $\beta\text{-CuZn}$ could be accessed in pH 14 electrolytes. The constant current dealloying methodology established here has provided fundamental insights into the mechanism of the EIPT. The materials produced by our method are scalable, which can enable integration into architectures for use in electrolyzers, plasmonic light absorbers, or other applications which can make use of intermetallic materials with controllable structures and compositions.

ASSOCIATED CONTENT

Supporting Information

The Supporting Information is available free of charge at https://pubs.acs.org/doi/10.1021/acs.chemmater.1c01678.

XRD patterns, SEM images, XPS images, ICP-MS results, and voltage-time curve (PDF)

AUTHOR INFORMATION

Corresponding Author

Anthony Shoji Hall — Department of Materials Science and Engineering, Johns Hopkins University, Baltimore, Maryland 21218, United States; Department of Chemistry, Johns Hopkins University, Baltimore, Maryland 21218, United States; orcid.org/0000-0003-4134-4160; Email: shoji@jhu.edu

Author

Yunfei Wang — Department of Materials Science and Engineering, Johns Hopkins University, Baltimore, Maryland 21218, United States; orcid.org/0000-0002-9684-1730

Complete contact information is available at: https://pubs.acs.org/10.1021/acs.chemmater.1c01678

Notes

The authors declare no competing financial interest.

■ ACKNOWLEDGMENTS

We gratefully thank the McQueen Lab and PARADIM at Johns Hopkins University for assistance with the XRD measurements, Professor Howard Fairbrother at JHU for assistance with the XPS measurement, and Maggie LaCourse at University of Maryland, Baltimore County, for assistance with ICP-MS measurements. A.S.H. acknowledges financial support from the National Science Foundation under award no. DMR-2047019.

REFERENCES

- (1) Park, G. O.; Yoon, J.; Shon, J. K.; Choi, Y. S.; Won, J. G.; Park, S. B.; Kim, K. H.; Kim, H.; Yoon, W.-S.; Kim, J. M. Discovering a Dual-Buffer Effect for Lithium Storage: Durable Nanostructured Ordered Mesoporous Co-Sn Intermetallic Electrodes. *Adv. Funct. Mater.* **2016**, 260, 2800–2808.
- (2) Wang, X.-L.; Feygenson, M.; Chen, H.; Lin, C.-H.; Ku, W.; Bai, J.; Aronson, M. C.; Tyson, T. A.; Han, W.-Q. Nanospheres of a New Intermetallic FeSn5 Phase: Synthesis, Magnetic Properties and Anode Performance in Li-ion Batteries. *J. Am. Chem. Soc.* **2011**, *133*, 11213–11219.
- (3) Kim, M. S.; Deepika; Lee, S. H.; Kim, M.-S.; Ryu, J.-H.; Lee, K.-R.; Archer, L. A.; Cho, W. I. Enabling reversible redox reactions in electrochemical cells using protected LiAl intermetallics as lithium metal anodes. *Sci. Adv.* 2019, *5*, No. eaax5587.

- (4) Tsai, A. P.; Kameoka, S.; Nozawa, K.; Shimoda, M.; Ishii, Y. Intermetallic: A Pseudoelement for Catalysis. *Acc. Chem. Res.* **2017**, 50, 2879–2885.
- (5) Furukawa, S.; Komatsu, T. Intermetallic Compounds: Promising Inorganic Materials for Well-Structured and Electronically Modified Reaction Environments for Efficient Catalysis. ACS Catal. 2016, 7, 735–765.
- (6) Rößner, L.; Armbrüster, M. Electrochemical Energy Conversion on Intermetallic Compounds: A Review. ACS Catal. 2019, 9, 2018–2062
- (7) Xiao, W.; Lei, W.; Gong, M.; Xin, H. L.; Wang, D. Recent Advances of Structurally Ordered Intermetallic Nanoparticles for Electrocatalysis. *ACS Catal.* **2018**, *8*, 3237–3256.
- (8) van den Berg, R.; Prieto, G.; Korpershoek, G.; van der Wal, L. I.; van Bunningen, A. J.; Lægsgaard-Jørgensen, S.; de Jongh, P. E.; de Jong, K. P. Structure sensitivity of Cu and CuZn catalysts relevant to industrial methanol synthesis. *Nat. Commun.* **2016**, *7*, 13057.
- (9) Yang, Y.; Xiao, W.; Feng, X.; Xiong, Y.; Gong, M.; Shen, T.; Lu, Y.; Abruña, H. D.; Wang, D. Golden Palladium Zinc Ordered Intermetallics as Oxygen Reduction Electrocatalysts. *ACS Nano* **2019**, 13, 5968–5974.
- (10) Varzi, A.; Mattarozzi, L.; Cattarin, S.; Guerriero, P.; Passerini, S. 3D Porous Cu—Zn Alloys as Alternative Anode Materials for Li-Ion Batteries with Superior Low T Performance. *Adv. Energy Mater.* **2018**, *8*, 1701706.
- (11) Kim, D.-M.; Cho, S. J.; Cho, C.-H.; Kim, K. B.; Kim, M.-Y.; Shim, Y.-B. Disposable all-solid-state pH and glucose sensors based on conductive polymer covered hierarchical AuZn oxide. *Biosens. Bioelectron.* **2016**, *79*, 165–172.
- (12) Su, Y.; Cockerill, I.; Wang, Y.; Qin, Y.-X.; Chang, L.; Zheng, Y.; Zhu, D. Zinc-Based Biomaterials for Regeneration and Therapy. *Trends Biotechnol.* **2019**, *37*, 428–441.
- (13) Maligal-Ganesh, R. V.; Xiao, C.; Goh, T. W.; Wang, L.-L.; Gustafson, J.; Pei, Y.; Qi, Z.; Johnson, D. D.; Zhang, S.; Tao, F.; Huang, W. A Ship-in-a-Bottle Strategy To Synthesize Encapsulated Intermetallic Nanoparticle Catalysts: Exemplified for Furfural Hydrogenation. ACS Catal. 2016, 6, 1754–1763.
- (14) Qi, Z.; Xiao, C.; Liu, C.; Goh, T. W.; Zhou, L.; Maligal-Ganesh, R.; Pei, Y.; Li, X.; Curtiss, L. A.; Huang, W. Sub-4 nm PtZn Intermetallic Nanoparticles for Enhanced Mass and Specific Activities in Catalytic Electrooxidation Reaction. *J. Am. Chem. Soc.* **2017**, *139*, 4762–4768
- (15) Cable, R. E.; Schaak, R. E. Solution Synthesis of Nanocrystalline M–Zn (M = Pd, Au, Cu) Intermetallic Compounds via Chemical Conversion of Metal Nanoparticle Precursors. *Chem. Mater.* **2007**, *19*, 4098–4104.
- (16) Marbella, L. E.; Andolina, C. M.; Smith, A. M.; Hartmann, M. J.; Dewar, A. C.; Johnston, K. A.; Daly, O. H.; Millstone, J. E. Gold-Cobalt Nanoparticle Alloys Exhibiting Tunable Compositions, Near-Infrared Emission, and High T2 Relaxivity. *Adv. Funct. Mater.* **2014**, 24, 6532–6539.
- (17) Bard, A. J.; Parsons, R.; Jordan, J.; International Union of Pure and Applied Physics. *Standard Potentials in Aqueous Solution*; M. Dekker: New York, 1985.
- (18) Schütte, K.; Meyer, H.; Gemel, C.; Barthel, J.; Fischer, R. A.; Janiak, C. Synthesis of Cu, Zn and Cu/Zn brass alloy nanoparticles from metal amidinate precursors in ionic liquids or propylene carbonate with relevance to methanol synthesis. *Nanoscale* **2014**, *6*, 3116–3126.
- (19) Ashberry, H. M.; Gamler, J. T. L.; Unocic, R. R.; Skrabalak, S. E. Disorder-to-Order Transition Mediated by Size Refocusing: A Route toward Monodisperse Intermetallic Nanoparticles. *Nano Lett.* **2019**, *19*, 6418–6423.
- (20) Sun, D.; Wang, Y.; Livi, K. J. T.; Wang, C.; Luo, R.; Zhang, Z.; Alghamdi, H.; Li, C.; An, F.; Gaskey, B.; Mueller, T.; Hall, A. S. Ordered Intermetallic Pd3Bi Prepared by an Electrochemically Induced Phase Transformation for Oxygen Reduction Electrocatalysis. ACS Nano 2019, 13, 10818–10825.

- (21) Geng, K.; Liu, M.; Xie, Y.; Aiello, A.; Karasz, E.; Sieradzki, K. Morphology Evolution during Delithiation of Li-Pb Alloys: Oscillatory Electrochemical Behavior. *J. Electrochem. Soc.* **2019**, *166*, C108–C114.
- (22) Chen, Q.; Sieradzki, K. Spontaneous evolution of bicontinuous nanostructures in dealloyed Li-based systems. *Nat. Mater.* **2013**, *12*, 1102.
- (23) Ballesteros, J. C.; Gomez-Solis, C.; Torres-Martínez, L. M.; Juárez-Ramírez, I. Electrodeposition of Cu-Zn Intermetallic Compounds for Its Application as Electrocatalyst in the Hydrogen Evolution Reaction. *Int. J. Electrochem. Sci.* **2015**, *10*, 2892–2903.
- (24) de Almeida, M. R. H.; Barbano, E. P.; Zacarin, M. G.; de Brito, M. M.; Tulio, P. C.; Carlos, I. A. Electrodeposition of CuZn films from free-of-cyanide alkaline baths containing EDTA as complexing agent. *Surf. Coat. Technol.* **2016**, *287*, 103–112.
- (25) Das, S.; Jena, S.; Banthia, S.; Mitra, A.; Das, S.; Das, K. Novel pulse potentiostatic electrodeposition route for obtaining pure intermetallic CuSZn8-CuZn composite coating using glycerol-NaOH based electrolyte with advanced scratch resistance and anticorrosive properties. J. Alloys Compd. 2019, 792, 770–779.
- (26) Cu (Copper) Binary Alloy Phase Diagrams. In *Alloy Phase Diagrams*; Okamoto, H., Schlesinger, M. E., Mueller, E. M., Eds.; ASM International, 2016; Vol. 3.
- (27) Zhang, X.; Van Hulzen, M.; Singh, D. P.; Brownrigg, A.; Wright, J. P.; Van Dijk, N. H.; Wagemaker, M. Direct view on the phase evolution in individual LiFePO4 nanoparticles during Li-ion battery cycling. *Nat. Commun.* **2015**, *6*, 8333.
- (28) Bai, P.; Cogswell, D. A.; Bazant, M. Z. Suppression of phase separation in LiFePO(4) nanoparticles during battery discharge. *Nano Lett.* **2011**, *11*, 4890–4896.
- (29) Mourdikoudis, S.; Liz-Marzán, L. M. Oleylamine in Nanoparticle Synthesis. *Chem. Mater.* **2013**, 25, 1465–1476.
- (30) Gilroy, K. D.; Ruditskiy, A.; Peng, H.-C.; Qin, D.; Xia, Y. Bimetallic Nanocrystals: Syntheses, Properties, and Applications. *Chem. Rev.* **2016**, *116*, 10414–10472.
- (31) Yan, Y.; Du, J. S.; Gilroy, K. D.; Yang, D.; Xia, Y.; Zhang, H. Intermetallic Nanocrystals: Syntheses and Catalytic Applications. *Adv. Mater.* **2017**, *29*, 1605997.
- (32) He, M.; Protesescu, L.; Caputo, R.; Krumeich, F.; Kovalenko, M. V. A General Synthesis Strategy for Monodisperse Metallic and Metalloid Nanoparticles (In, Ga, Bi, Sb, Zn, Cu, Sn, and Their Alloys) via in Situ Formed Metal Long-Chain Amides. *Chem. Mater.* **2015**, *27*, 635–647.
- (33) Endres, F. Ionic Liquids: Solvents for the Electrodeposition of Metals and Semiconductors. *ChemPhysChem* **2002**, *3*, 144–154.

■ NOTE ADDED AFTER ASAP PUBLICATION

This paper was published ASAP on September 8, 2021, with an error in the Figure 3 caption. The corrected version was reposted on September 28, 2021.